RESEARCH TRIANGLE INSTITUTE

ENGINEERING STUDIES RELATED TO GEODETIC AND OCEANOGRAPHIC REMOTE SENSING USING SHORT PULSE TECHNIQUES

Final Engineering Report

For Task D

May 1973

Prepared Under

NASA CONTRACT NO. NAS6-2135

for

National Aeronautics and Space Administration

Wallops Station

Wallops Island, Virginia 23337

FORWARD

This report was prepared for the National Aeronautics and Space Administration by the North Carolina State University on a sub-contract from Research Triangle Institute under contract NAS6-2135. Messrs. J. T. McGoogan and H. R. Stanley of NASA/Wallops Station acted as technical coordinators of the contract.

The study was performed by the Departments of Geosciences and Engineering Mechanics of NCSU. The project staff consisted of Professors N. E. Huang (Project Leader), F. Y. Sorrell (Consultant) and C. C. Tung (Consultant) with Messrs. S. R. Long and G. V. Sturm participating as research assistants. Mr. K. L. Fan also contributed to the last phase of the study.

ABSTRACT

This report presents the theoretical basis for a feasibility study of measuring global ocean surface current pattern from satellites and aircraft. The analysis is supported by some preliminary laboratory experiments. Since the ultimate goal of the study is to establish an operational routine for monitoring the global current pattern, a non-disturbing remote sensing device using a laser probe was developed. Detailed construction of the measuring system and the results of some preliminary observations are also presented. Future plans are also briefly discussed.

CONTENTS

INTRODUCTION

This report presents the results of a feasibility study on the measurement of surface current patterns from satellites and aircraft. The theoretical principle is based on current-wave interactions and the resulting modification of waves by any concurring current. In order to carry out some laboratory observations as a first check of the analysis, a new non-disturbing laser probe for wave measurement was built. Some preliminary results are presented to support the theoretical analysis. The report consisted of the following chapters.

Chapter 2 presents the main theoretical basis for the study. The analysis was made for both gravity and capillary wave ranges. Two approaches were presented for possible applications. The first one is based on wave kinematies, and laboratory observations confirm the accuracy of this approach. The second approach is based on dynamics. Both of these analyses were published by Huang et al. (1972).

Chapter 3 describes the experimental techniques and also details some of the results, including both the principles of the design, error analysis of the system, the description of the actual system, and some preliminary results on wave kinematics. The future plans are also discussed with a detailed description of a two-dimensional wave measuring device constructed during the period of this study for test in the next phase of fully wind generated waves interacting with currents.

The final chapter discusses briefly the future plans for the study.

2.0 THEORETICAL ANALYSIS

Since surface waves belong to a special class of motion in which the fluid particles are organized in a particular way, any concurrent motion will introduce interactions. Through such interactions, the wave characteristics will be modified; therefore, by careful measurements of the waves, we can deduce the current information. Ultimately, we can use wave observation as a way of current measurements. There are two general approaches to the ultimate goal of current measurements. The first approach is based on the kinematic conservation law and the second one is by the dynamical conservation laws of the waves. The basic analysis will be presented below.

2.1 Kinematic Approach

Let a component of a general wave field be specified by

$$\zeta(\underset{\sim}{x},t) = a(\underset{\sim}{x},t)\ e^{iX(\underset{\sim}{x},t)} \tag{2-1}$$

where $\zeta(\underset{\sim}{x},t)$ is the surface elevation at position $\underset{\sim}{x}$ and time t, $a(\underset{\sim}{x},t)$ is the amplitude function and $X(\underset{\sim}{x},t)$ the phase function. The wave number $\underset{\sim}{k}$ and the frequency n can be defined by

$$\left.\begin{aligned} \underset{\sim}{k} &= \nabla X \\ n &= -\frac{\partial X}{\partial t} \end{aligned}\right\} \tag{2-2}$$

Combining the two expansions in equation (2-2), we have the kinematic conservation law of the waves

$$\frac{\partial \underset{\sim}{k}}{\partial t} + \nabla n = 0 \tag{2-3}$$

This frequency is called the total frequency by Huang et al. (1972), and is also the frequency one actually observes. When the waves encounter currents, the total frequency becomes

$$n = \underset{\sim}{k} \cdot \underset{\sim}{U}(\underset{\sim}{x},t) + \sigma \tag{2-4}$$

where σ is the oscillatory frequency of the wave motion alone. Under a steady state condition, a generalized dispersion relation can be found. For pure gravity waves we have

$$gk = \frac{n^2}{\left[\frac{1}{2} + \frac{1}{2}\left(1 + \frac{4U\,n}{g}\right)^{1/2}\right]^2} \tag{2-5}$$

A comparison with existing data by Francis and Dugeon (1967) and Plate and Trawle (1970) was made and the agreement is very good as shown in Figure 2-1.

When the influence of capillary force is considered, we have

$$C^2 = C_o^2 \left(\frac{k_o}{k}\right)^2 + U^2 - 2U\,C_o \left(\frac{k_o}{k}\right) \tag{2-6}$$

where C and k are phase speed and wave number of a wave under the influence of a current while the subscript o indicates the condition when the current U = 0. The result is presented in Figure 2-2.

The advantage of adopting this kinematic approach is that we can get the absolute current by any local measurement. However, the difficulty is with the data acquisition; we need measurements on wave number and frequency simultaneously. Due to this limitation, we developed an alternate approach.

2.2 Dynamic Approach

In this approach, we use the energy conservation equation. For the one dimensional case under steady state conditions, the energy equation can be written as in Phillips (1966):

$$E\left(\frac{C}{2} + U\right) C = \frac{1}{2} E_o C_o^2 = \text{constant} \tag{2-7}$$

From this relation, the energy spectrum can be calculated by using the current velocity U as a parameter as shown in Huang et al. (1972). Since the radar altimeter technique depends on the mean back scattering cross section of the surface which, in turn, depends on the mean surface slope; the

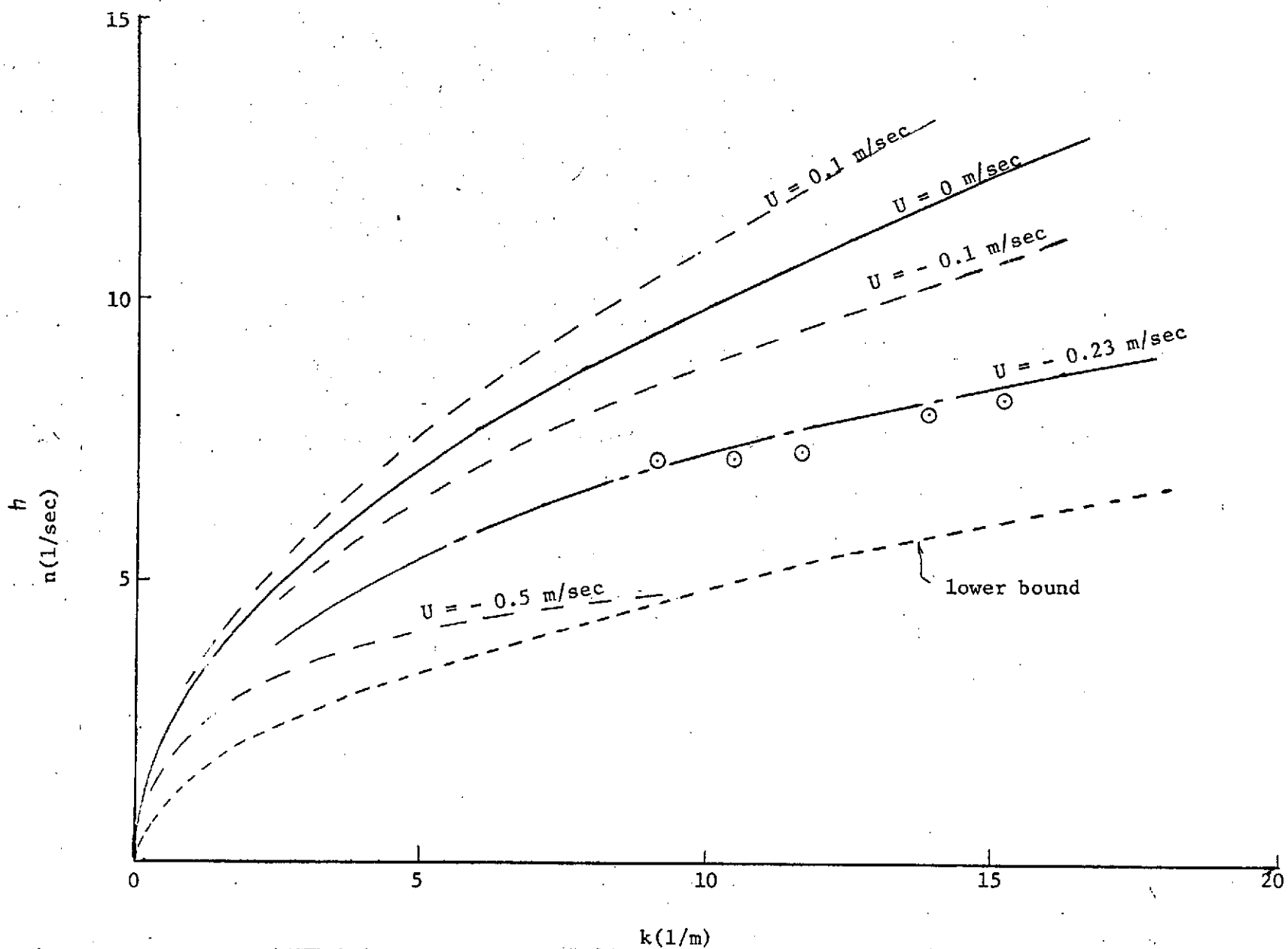

Figure 2-1. Influence of current on the dispersion relationship. The dotted line ----- corresponds to the limiting condition when the group velocity equals, -U, and ⊙ are laboratory observations by Plate and Trawle (1970).

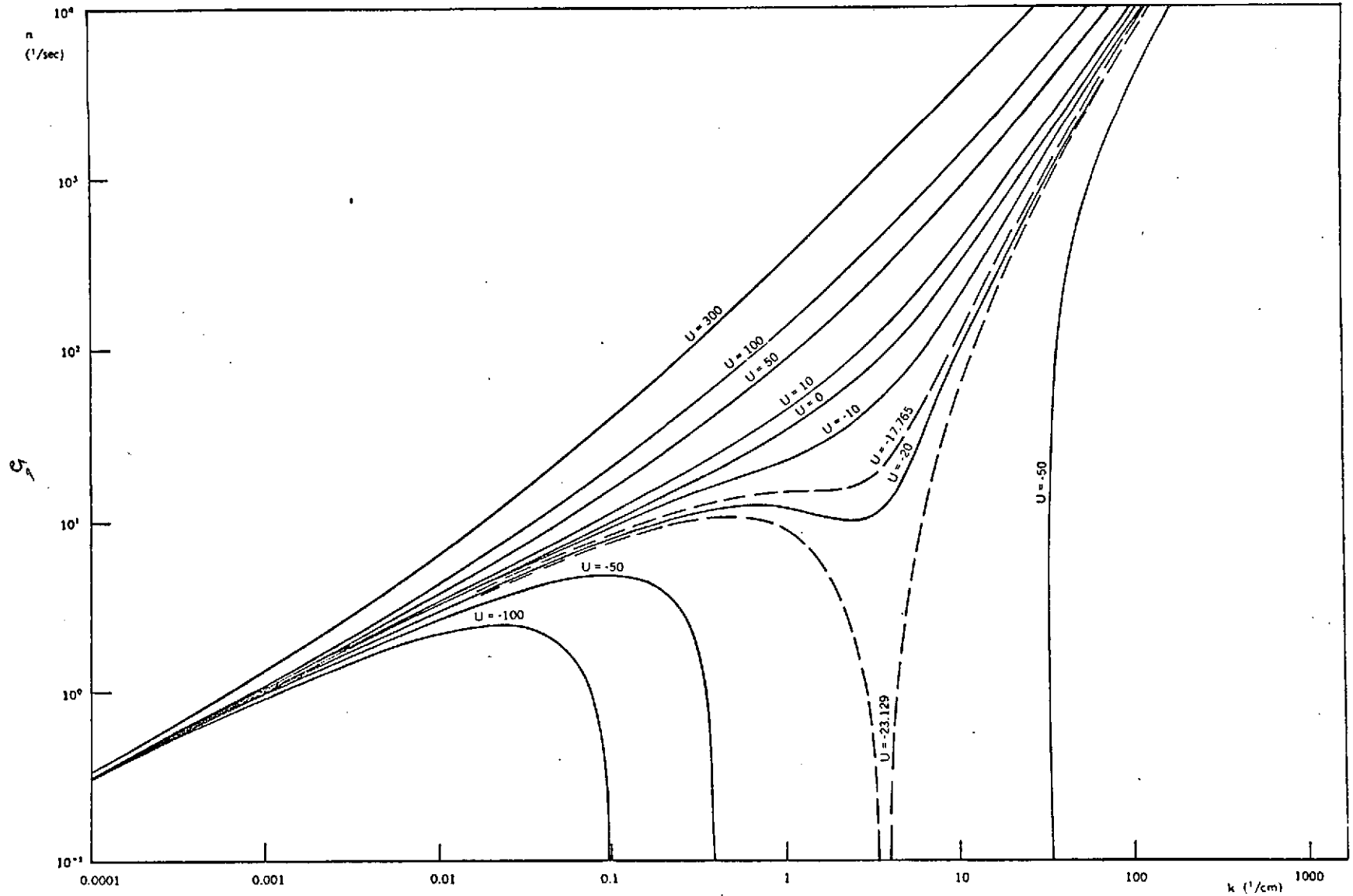

Figure 2-2. Influence of current on the dispersion relationship for gravity-capillary waves.

surface slope spectrum then becomes a crucial quantity for remote sensing measurements. It can be shown (see, for example, Phillips, 1966) that the surface slope spectrum $S_{\alpha\beta}(\underset{\sim}{k},n)$ is related to the surface elevation spectrum $X(\underset{\sim}{k},n)$ by

$$S_{\alpha\beta}(\underset{\sim}{k},n) = K_\alpha K_\beta X(\underset{\sim}{k},n) \tag{2-8}$$

In particular, when $\alpha = \beta = 1$, say, we have

$$S_{11}(\underset{\sim}{k},n) = k^2 X(\underset{\sim}{k},n) \tag{2-9}$$

If $X(k,n)$ depends on current U, so will $S_{11}(\underset{\sim}{k},n)$. Thus the mean square surface slope

$$\overline{(\nabla\zeta)^2} = \int_{\underset{\sim}{k}} \int_n S_{11}(\underset{\sim}{k},n)\, d\underset{\sim}{k}\, dn = \int_{\underset{\sim}{k}} \int_n \underset{\sim}{k}^2 X(\underset{\sim}{k},n)\, d\underset{\sim}{k}\, dn \tag{2-10}$$

is also a function of current velocity. The relation between mean square surface slope and the current is established through numerically integrating equation (2-10) with current U as a parameter in $X(\underset{\sim}{k},n)$. The results are shown in Figure 2-3.

The advantage of this dynamic approach is in the simplicity of data acquisition, i.e. existing radar measurement techniques are nearly sufficient. However, since the dynamics approach is based on velocity change, it can only give relative values of current changes. Furthermore, the energy of every wave eventually will be dissipated over a long range of propagation. Therefore, in order that the waves will experience a substantial velocity gradient during this iife time, the current gradient must be very strong. All this limits the usefulness of this approach to such cases as flow through tidal inlets in coastal region or the well defined major ocean current systems such as Gulf Stream and Kuroshio.

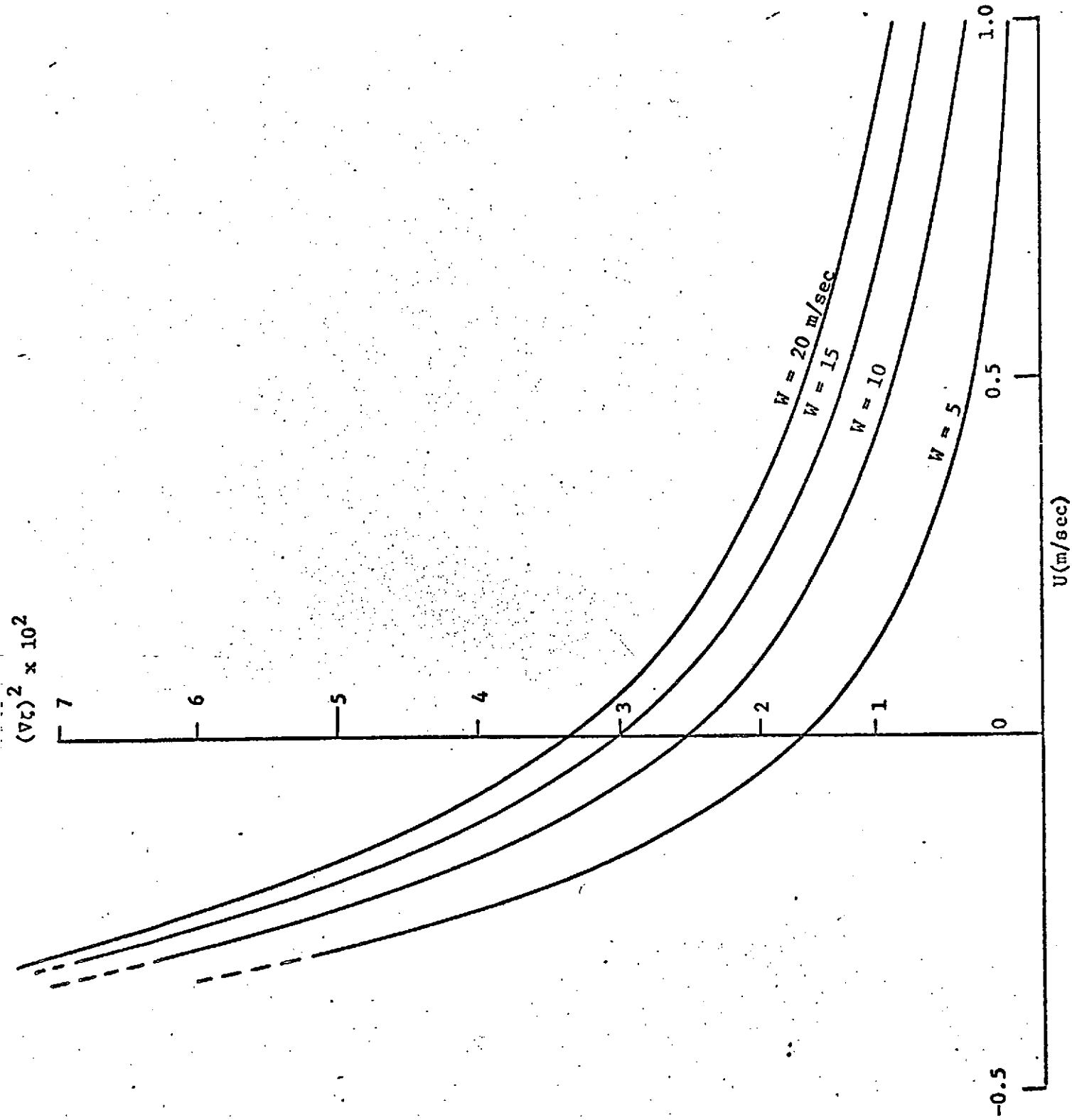

Figure 2-3. Variation of rms surface slope with current speed with wind speed as a parameter.

3.0 EXPERIMENTAL STUDIES

Although much of the surface energy of the ocean is contained in long, large amplitude waves, there are many situations in which surface slope or surface roughness is important such as the case in the present study of using a radar altimeter for a study of sea state properties. Waves to which the radar altimeter typically are sensitive have greater slopes or higher values of ak (amplitude-wavenumber product), than the longer gravity waves. Although the ultimate laboratory test will be run in a wind-wave tank, the capillary waves were selected for this preliminary study for the following reasons:

(1) Microwave radiation reflected from the ocean surface depends greatly on the high wave number range of the spectrum. Therefore even in the full wind-wave study we still have to understand the importance of the capillary wave range.

(2) In this high wavenumber range the phase speed is low. Since the influence of current on waves is measured by the ratio of current speed to phase speed, the gravity-capillary wave is, therefore, most susceptible to the influence of currents.

(3) In this range, the wave length is relatively short therefore it is easily reproduced in a small tank for testing the validity of the theoretical analyses.

This chapter describes a technique that permits the measurement of gravity-capillary waves to an accuracy not previously possible. The requirements of such a wave measurement system are spatial resolution on the order of a fraction of a millimeter, flat frequency response from 2 to 40 Hertz, and a minimum of surface disturbance. The latter is important as the meniscus on a probe can cause errors in height measurement and the probe itself may alter the wave as it passes by generating spurious waves. Because of these requirements an optical measurement system was deemed desirable. The system described in this chapter utilizes a small diameter light beam directed vertically through the surface such that the angle the beam is refracted by the sloped surface can be measured by a photodetector. Such a system gives a spatial resolution equal to the light beam diameter, typically 0.25 to 0.50 mm, and a frequency response equal to that of the electronics used to detect the angle of refraction. In addition, the system obviously creates no surface disturbance. Such a technique is primarily a surface slope measurement.

In situations where longer, lower frequency waves are to be measured, a wave height probe can be conveniently utilized. These devices, which convert the immersion depth of a slender probe to an analog voltage, have simplicity and read wave height directly; however, results reported here indicate that the meniscus effect can cause some measurement errors at short wavelengths. Moreover, when a mean flow is present, due either to a current or a long wave, the probe can produce additional waves, typically capillary or gravity-capillary waves of the type that are being investigated. Because these wave height probes have been used over a wide range of application, a careful comparison of results from the wave height probe with those taken by the optical system was made.

Previous attempts to measure surface slopes by optical means can be loosely divided into two categories: (1) those based on reflection and (2) those based on refraction. Early reflective techniques were confined to the analysis of sun glitter photographs. Hulburt (1934) related the width of the sun path as viewed through plane polarizers to the maximum slope of surface facets on the Atlantic. Later Cox and Munk (1954) obtained large area glitter photographs with airborne cameras. Whereas Hulburt calbulated only the maximum surface slopes as a function of sun path width, Cox and Munk calculated the distribution of mean-square surface slopes from emulsion density measurements of the sun glitter photographs.

Schooley (1954) elaborated somewhat on the glitter technique by substituting flashbulbs for the light source. Using this technique river slope spectra were correlated with wind velocities.

Later, Cox (1958) utilized refraction rather than reflection to study the slope of wind and plunger generated waves in a small laboratory wave channel. Light passed through a linear density transmission filter, entered through the bottom of the wave channel, and was refracted at the air-water interface and collected by a telescope-photodetector. Variations in surface slope were related to the intensity variation of the light bundle intercepted by the telescope. Unfortunately, the brightness due to changes in slope was not constant but varied as much as $\pm$ 20% for slopes measured near the peaks or troughs of large amplitude waves. In addition, cross wave slopes, scattered light, and possible variations in brightness due to internal reflections were collectively registered by the phototube and as such could not be separated from variations in brightness due to slope. However, high spatial resolution was obtained by this system as Cox estimated the light beam diameter (effective sensor size) to be 0.7 mm.

3.1 Experimental Technique

The optical technique used in the present investigation employs the refraction of a narrow beam of light at the air-water interface. Figure 3-1 illustrates an idealization of a one-dimensional wave as traversed by the incident light beam.

The light beam enters vertically from below and intercepts the surface which has the instantaneous slope $d\zeta/dx = \tan\theta_1$ at the angle θ_1 with respect to the surface normal. As a result of refraction the beam enters the air at angle θ_2 with respect to the same normal. Angles θ_1, θ_2 and indices of refraction n_1 and n_2 are related by Snell's law of refraction, $n_1 \sin\theta_1 = n_2 \sin\theta_2$. Since θ_1 and θ_2 are measured from the surface normal, the difference angle $\alpha = \theta_2 - \theta_1$ or simply the angular deviation from the vertical is measured experimentally. The difference angle α can be related to the angle θ_1 through Snell's law to give

$$\cot\theta_1 = \frac{n_1}{n_2}\csc\alpha - \cot\alpha \qquad (3\text{-}1)$$

The surface slope, $d\zeta/dx = \tan\theta_1$, is simply the reciprocal of Eq. (3-1). Hence, by a measurement of α one can obtain the instantaneous surface slope at the point traversed by the light beam. Equation (3-1) is valid for any wave slope as long as θ_1 is less than the critical angle, θ_c, where total internal reflection occurs. In order to measure the difference angle α one relates the offset distance d of the refracted beam from the vertical to the distance ℓ of the disturbed surface to the photodetector as simply $\alpha = a\tan(d/\ell)$. When $\ell >> a$ where a is the total vertical surface displacement, ℓ may be considered constant. The present system requires that ℓ be constant and thus for the method in its present form to be used for finite amplitude waves, the detector must be sufficiently far away that $\ell >> a$. This is the only restriction on wave amplitude that is inherent in the system, and for the present experiments a/ℓ was always less than 0.005. The difference angle α is given by the linear relationship $\alpha = d/\ell$ to an error less than 5% whenever $d/\ell < 0.30$. In these experiments the maximum value of d/ℓ used was 0.18. Detailed analysis is given in the following section.

In actual operation a beam of light from a Spectra-Physics model 132 laser is focused to a diameter of approximately 1/4 mm and directed vertically through the surface. The position of the light beam from the vertical, which

is shown as d in Figure (3-1), is measured by a United Detector model PIN-LSC-9 photodiode, as shown in Figure 3-2. This diode has an active area of 2.5 mm by 225 mm and produces a voltage proportional to the product of the incident light intensity and the distance of the incident position from some arbitrary position (usually this position is selected so the diode gives the product of intensity times d). The diode has a provision for separate monitoring of the incident light intensity. When intensity variations are present, the variation in intensity is removed by analog voltage division of the position times intensity voltage product by the intensity voltage. The analog voltage divider is constructed from a four-quadrant X-Y multiplier, which is described in integrated circuit product (e.g. Motorola, Signetics or Fairchild) handbooks. The quotient voltage thus obtained is linearly proportional to the offset distance, d, of the light spot. For most cases, with carefully skimmed tap water, the intensity of the refracted light beam is constant, and the diode output voltage is proportional to the offset distance and hence d. Thus the divider circuit is not required. When the lateral deviation of the light beam is greater than 2.5 mm (the width of the active area of the photodiode) a cylindrical lens is used to keep the light beam on the active area of the diode.

Having the position voltage proportional to distance d, the difference angle is obtained directly as

$$\alpha = \frac{e_{diode}}{D_s \ell} \quad , \tag{3-2}$$

where D_s is the diode position sensitivity in volts/cm and e_{diode} is the output voltage from the diode. Equation (3-1) may be linearized for small α and θ_1 whereby one obtains

$$\frac{d\zeta}{dx} = \tan \theta_1 \pm \frac{n_2}{n_1 - n_2} \alpha \quad . \tag{3-3}$$

Combining equations (3-2) and (3-3) one obtains the desired relationship between surface slope and output voltage

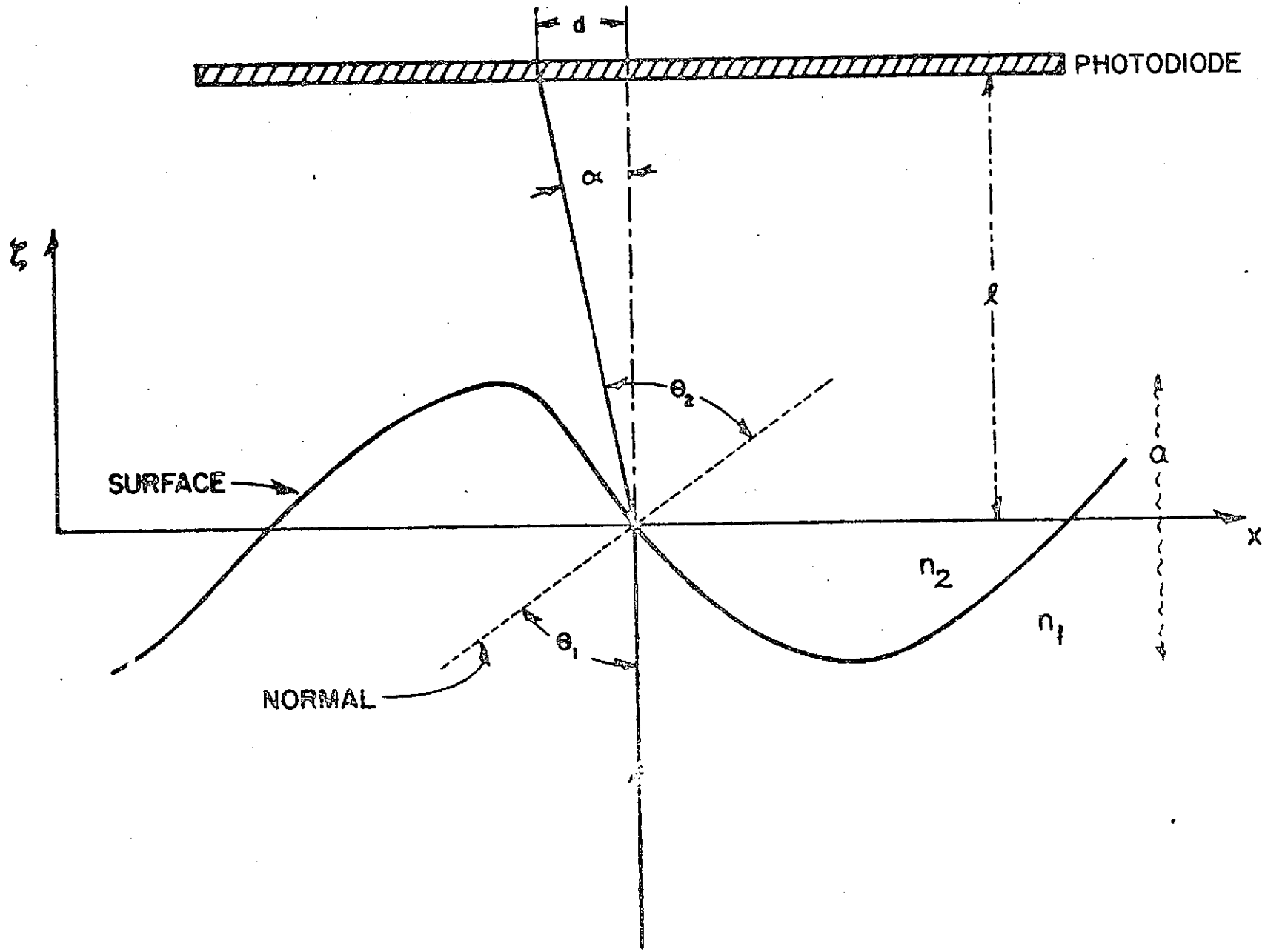

Figure 3-1. Optical path and refraction angles for a one dimensional wave.

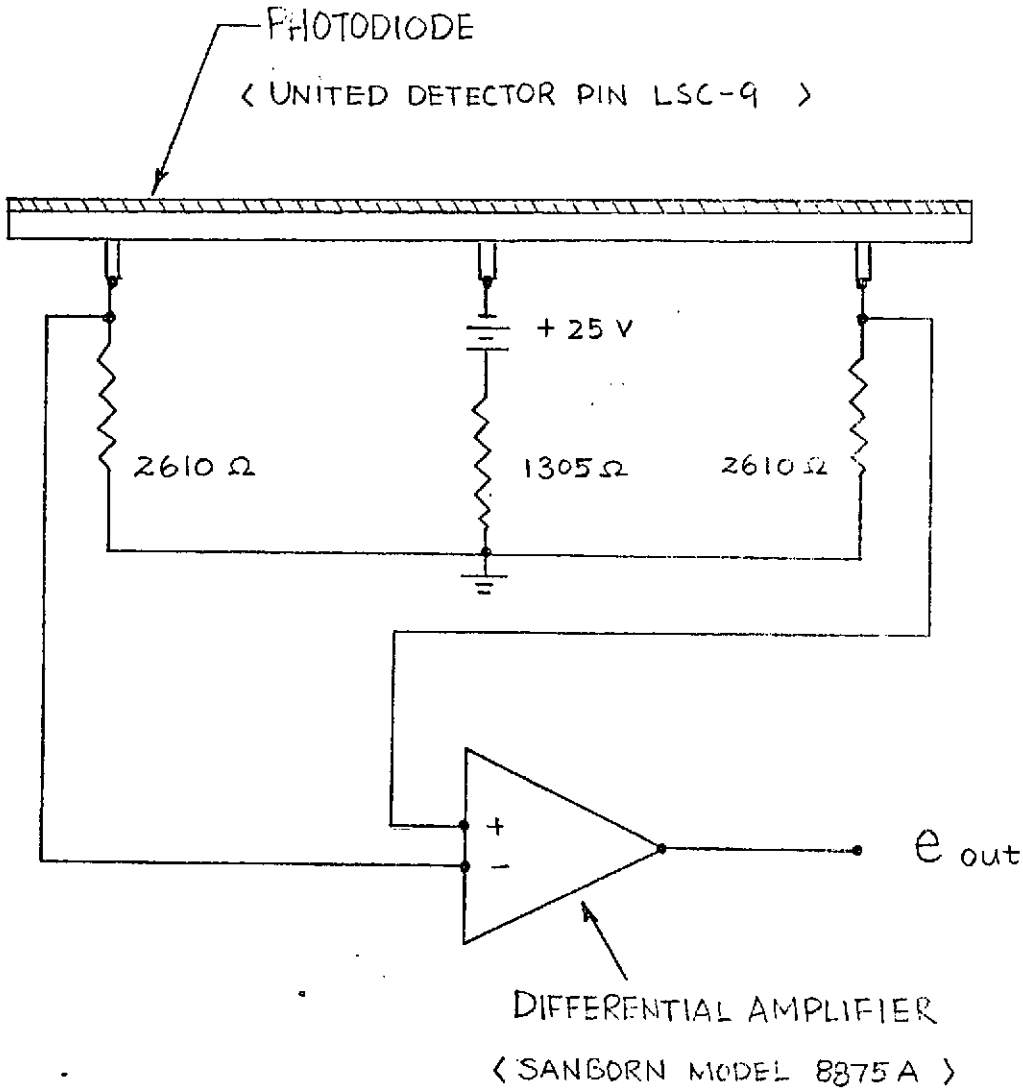

Figure 3-2. Circuit diagram for the photodiode and differential amplifier.

$$\frac{d\zeta}{dx} = \frac{n_2}{n_1 - n_2} \frac{e_{diode}}{D_s \ell} \tag{3-4}$$

For an air-water system Eq. (3-4) is accurate to within 5% when $\alpha < 0.18$.

Having obtained the wave slope as a function of time the wave height can be computed if the phase velocity is known. To illustrate this, for a steady one-dimensional wave propagating along the x-axis with phase velocity c, the instantaneous vertical velocity of the surface (for fixed x) is found as

$$\frac{d\zeta}{dt} = \frac{d\zeta}{dx}\frac{dx}{dt} = c\,\frac{d\zeta}{dx} \tag{3-5}$$

The surface height (at the same point) is simply

$$\zeta(t) = \int \left(\frac{d\zeta}{dt}\right) dt = \int c\,\frac{d\zeta}{dt}\, dt \tag{3-6a}$$

For this experiment the phase velocity was computed to change by less than 0.1% over a wavelength and no change over 10 wavelengths was ever measured (within experimental accuracy). For constant velocity c the integral reduces to

$$\zeta(t) = c \int \frac{d\zeta}{dx}\, dt \tag{3-6b}$$

The integration in Eq. (3-6b) can be performed by any electronic system that exhibits a transfer function of $e_{out} = b\int e_{in} dt$ where b is a constant. For the present investigation an operational amplifier with capacitive feedback was employed. With $d\zeta/dx$ given by Eq. (3-4) as input to the analog integrator one obtains

$$\zeta(t) = mc\, e_{out}$$

where $m = n_2(n_1 - n_2)^{-1}(D_s \ell b)^{-1}$ and e_{out} is the output voltage from the analog integrator. A block diagram of the system is given in Figure 3.3.

The experiments were conducted in a wave-tank constructed of acrylic plastic (Plexiglas) measuring 256 x 20 x 18 cm. The wave generator for the system is a 20° triangular plunger with the plunger shaft driven vertically by a larger permanent-magnet loudspeaker. The motion is monitored by a dc

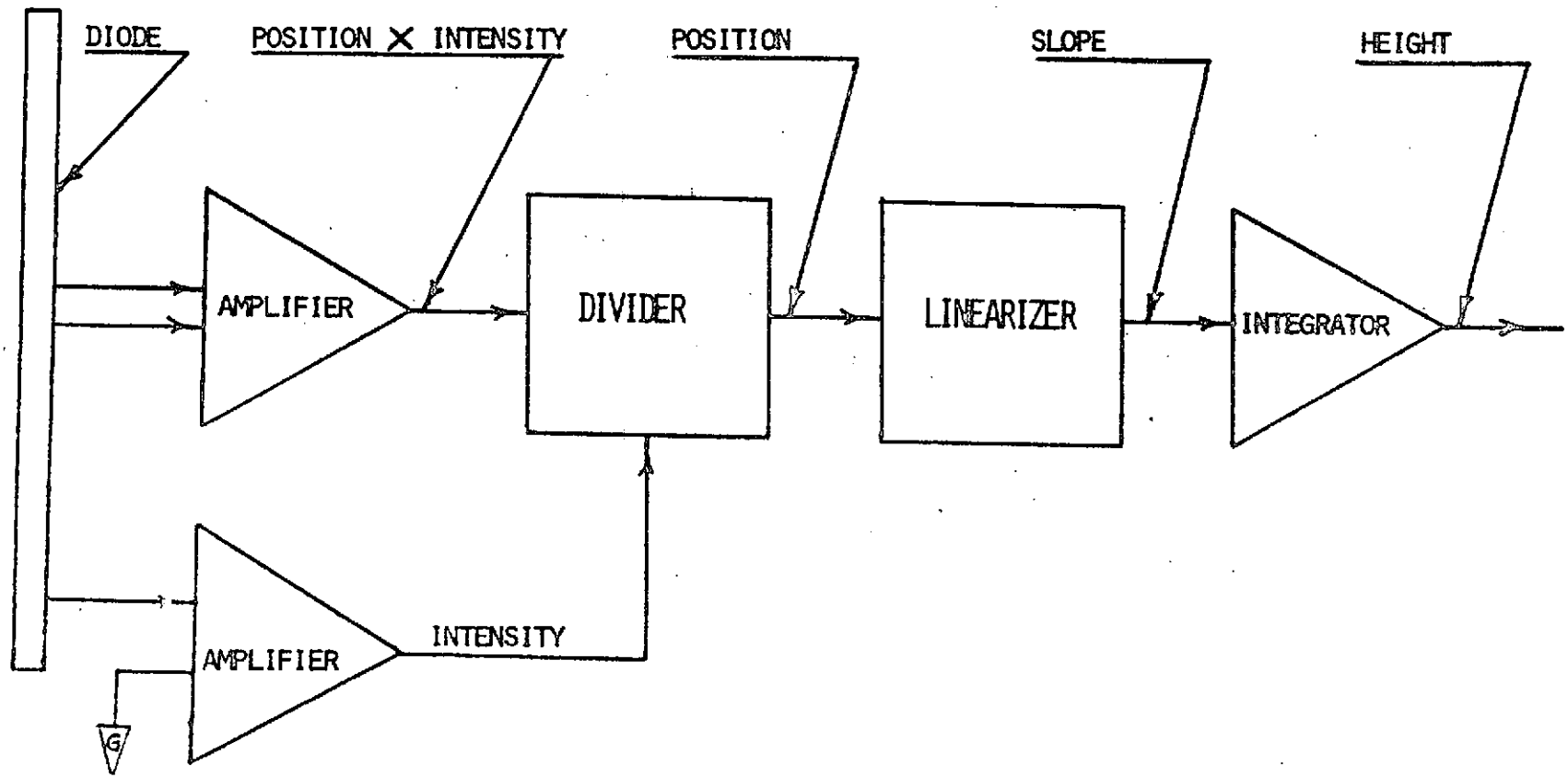

Figure 3-3. Schematic diagram for the one-dimensional wave sensor.

differential transformer (dcdt) which drives the error circuitry. The loudspeaker, dcdt, and error circuit comprise a feedback-controlled electromechanical transducer with controllable response characteristics. The power amplifier is of a complementary-symmetry transistor design such that one can obtain full power response down to dc. The laboratory set-up is shown in Figures 3–4 and 3–5.

3.2 Error Analysis Due to Surface Motion

Since the wave surface is constantly in motion, the reflection point is moving also, hence error may be introduced in the measurement process. To calculate the order of the error induced in this way we first examine the case of a single train of waves where the surface elevation $\zeta(x,t)$ is given as

$$\zeta(x,t) = a \sin(kx - \sigma t) = a \sin \chi \tag{3-7}$$

Let the distance between the mean water surface to the diode be H, then the instanteneous distance will be

$$h(t) = H + a \sin \chi \tag{3-8}$$

To the approximation of equation (3.6a), we have the apparent surface elevation $\zeta^*(x,t)$ as

$$\zeta^*(x,t) = \frac{1}{H}\int (H + a \sin \chi)\, ak \cos \chi \, dx \, \frac{\sigma}{k}$$

$$= a \sin \chi + \frac{a^2}{4H} \cos 2\chi \quad , \tag{3-9}$$

which results in an error on the order of

$$\frac{\varepsilon}{a} \alpha \frac{a}{4H}$$

In our study, $a \simeq 0.2$ cm, H = 100 cm. and the error is about 0.05%.

In the case of random wave field, the phase speed is hard to determine; therefore the surface elevation spectrum will have to be derived from the expression for the surface slope spectrum. Let the surface of the random wave

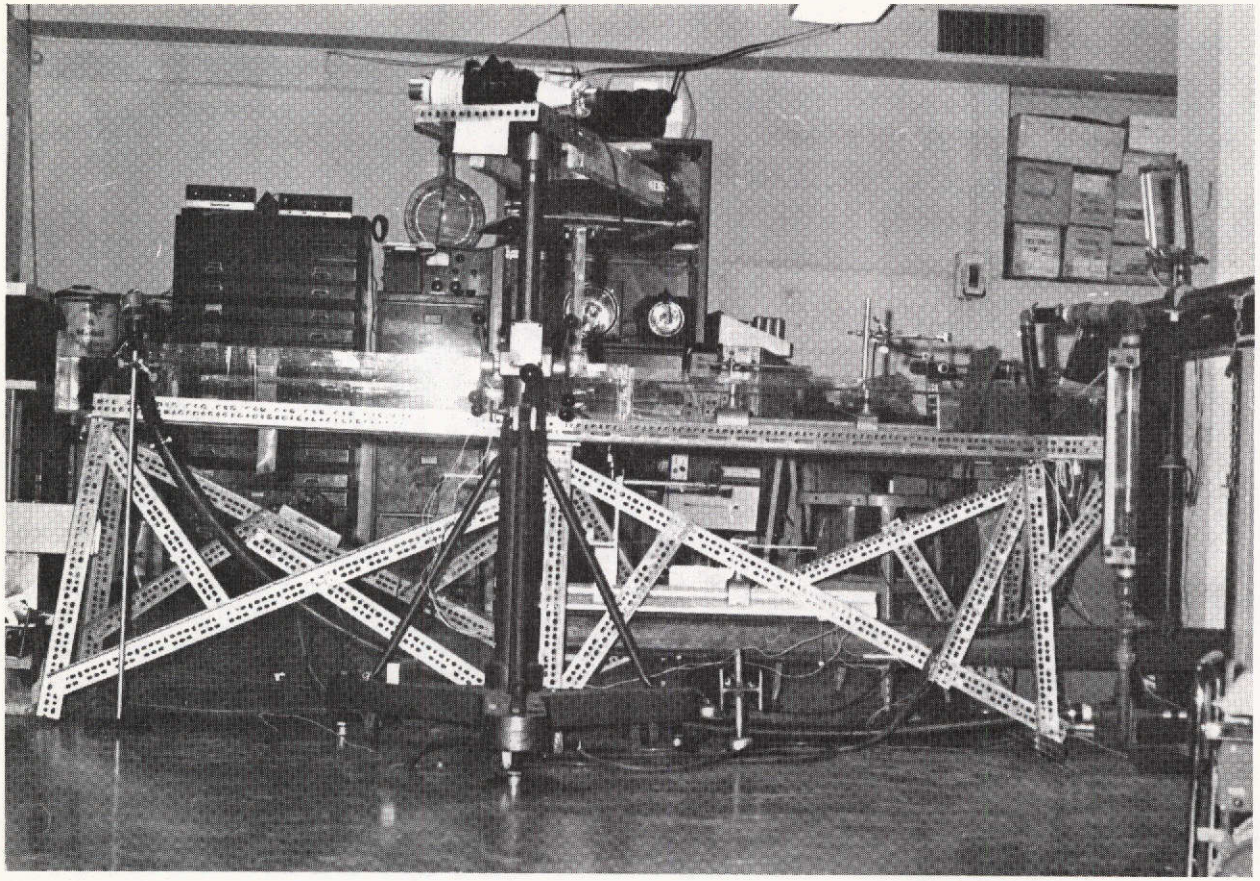

Figure 3-4. Laboratory set-up of the capillary-gravity wave tank.

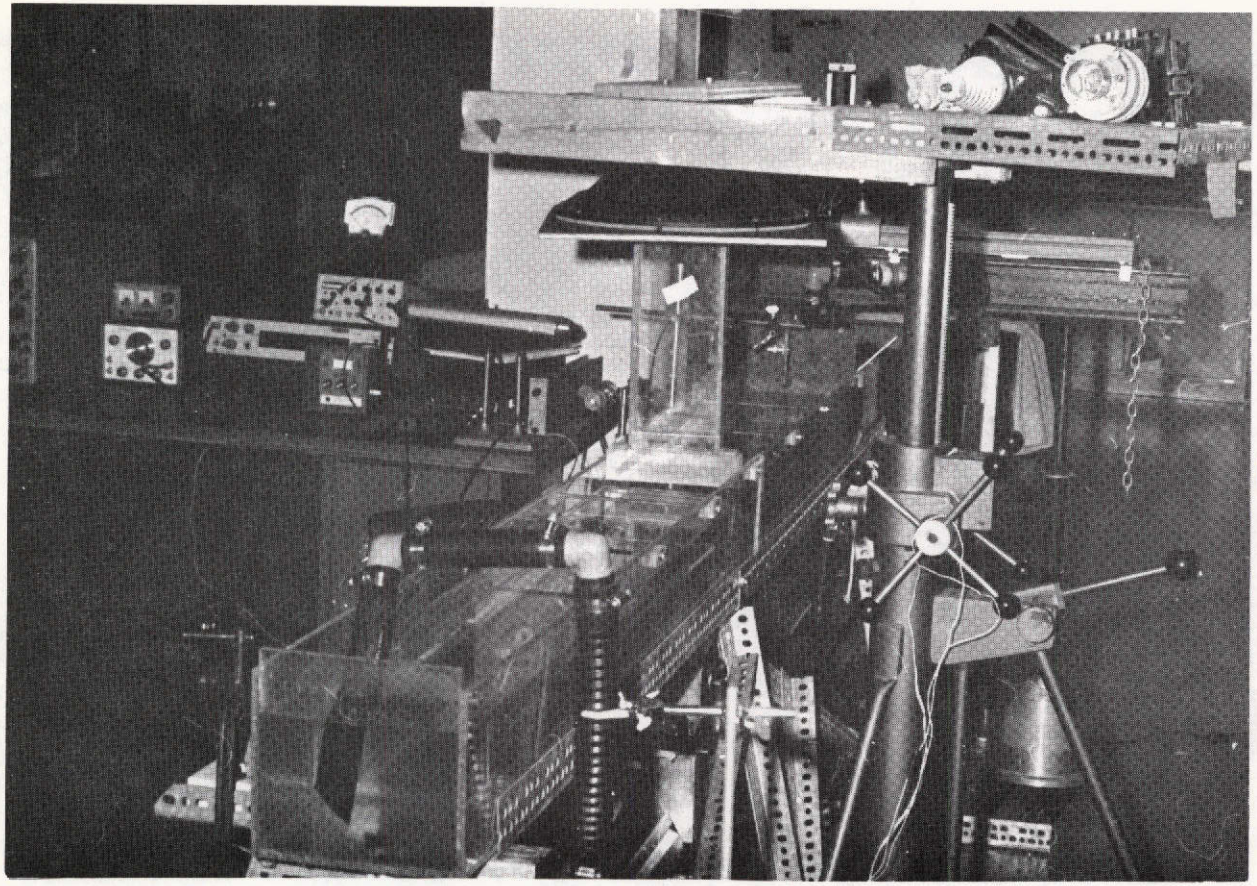

Figure 3-5. Close-up of tank, wave generator and some instruments.

field be expressed as

$$\zeta(\underset{\sim}{x},t) = \int_{\underset{\sim}{k}} \int_{n} dA(\underset{\sim}{k},n)\ e^{iX} \qquad (3\text{-}10)$$

with $dA(\underset{\sim}{k},n)$ as a complex valued random function which is related to the spectrum $X(k,n)$ by

$$\overline{dA(\underset{\sim}{k},n)\ dA^*(\underset{\sim}{k}_1,n_1)} = X(\underset{\sim}{k},n) \text{ if } \underset{\sim}{k} = \underset{\sim}{k}_1,\ n = n_1$$

$$= 0 \quad \text{if } \underset{\sim}{k} \neq \underset{\sim}{k}_1,\ n \neq n_1 \quad . \qquad (3\text{-}11)$$

The surface slope will be

$$\nabla\zeta(\underset{\sim}{x},t) = \int_{\underset{\sim}{k}} \int_{n} i\ \underset{\sim}{k}\ dA(\underset{\sim}{k},n)\ e^{iX} \quad . \qquad (3\text{-}12)$$

Thus the surface slope spectrum is

$$S_{ij}(\underset{\sim}{k},n) = \int_{\underset{\sim}{k}} \int_{n} k_i k_j\ X(\underset{\sim}{k},n)\ d\underset{\sim}{k}\ dn \qquad (3\text{-}13)$$

where k_i, k_j are the components of wave number in the ith and jth direction. For a one dimensional case $k_i = k_j = k$ and

$$S(k,n) = \int_{k} \int_{n} k^2\ X(k,n)\ dk\ dn \qquad (3\text{-}14)$$

Again, if the distance between the mean water level to the diode is given by H, the excursion of the light spot on the diode is

$$E(\underset{\sim}{x},t) = \left\{ H + \int_{\underset{\sim}{k}} \int_{n} dA(\underset{\sim}{k},n)\ e^{iX} \right\} \cdot \int_{\underset{\sim}{k}} \int_{n} \underset{\sim}{k}_1\ dA(\underset{\sim}{k}_1,n_1)\ e^{iX} \qquad (3\text{-}15)$$

The correlation function of this random position is

$$\overline{\underset{\sim}{E}(\underset{\sim}{x},t)\cdot\underset{\sim}{E}(\underset{\sim}{x}+\underset{\sim}{r},\ t+\tau)}$$

$$= \left\{ H + \int_{\underset{\sim}{k}}\int_{n} dA(\underset{\sim}{k},n)\ e^{iX} \right\} \cdot \int_{\underset{\sim}{k}_1}\int_{n_1} i\ \underset{\sim}{k}_1\ dA(\underset{\sim}{k}_1,n_1)\ e^{i\dot{X}1}$$

$$\cdot \left\{ H + \int_{\underset{\sim}{k}}\int_{n} dA^*(\underset{\sim}{k}_2,n_2)\ e^{-iX2} \right\} \cdot \int_{\underset{\sim}{k}_3}\int_{n_3} -i\ \underset{\sim}{k}_3\ dA^*(\underset{\sim}{k}_1,n_1) e^{-iX3} \qquad (3\text{-}16)$$

After some algebra, we have

$$\overline{\underset{\sim}{E}(\underset{\sim}{x},t)\cdot\underset{\sim}{E}(\underset{\sim}{x}+\underset{\sim}{r},\ t+\tau)}$$

$$= H^2 \int_{\underset{\sim}{k}}\int_{n} k_i k_j\ X(\underset{\sim}{k},n) \left\{ 1 + \frac{3}{H^2} \int_{\underset{\sim}{k}_1}\int_{n_1} \frac{\underset{\sim}{k}_1\cdot\underset{\sim}{k}_i}{k^2} \right.$$

$$\left. \cdot\ X(\underset{\sim}{k}_1,n_1)\ d\underset{\sim}{k}_1 dn_1 \right\}\ d\underset{\sim}{k}\ dn \qquad (3\text{-}17)$$

Comparing (3-17) with the true surface slope spectrum, we have an error of the order of

$$\frac{3}{H^2} \int_{\underset{\sim}{k}_1}\int_{n_1} \frac{\underset{\sim}{k}_1\cdot\underset{\sim}{k}_1}{k^2}\ X(\underset{\sim}{k}_1,n_1)\ d\underset{\sim}{k}_1\ dn_1 = 0\left(\frac{\overline{\zeta^2}}{H^2}\right) \qquad (3\text{-}18)$$

Although, the result is wave number dependent, its magnitude is small if $H^2 >> \overline{\zeta^2}$ which was the case in the set-up for experimental study.

3.3 Results of the Measurements

As indicated in Eq. (3-6) one must know the phase velocity before quantitative amplitude measurements on single trains of waves can be obtained. In theory, at least, it is a straightforward matter to obtain the phase velocity c from $c = f\lambda$, as λ can be measured experimentally and f, the wave (plunger) frequency, is known. However, for the short wavelengths encountered small

errors in measured wavelength will result in relatively large errors in phase velocity. In view of this a general dispersive relationship was sought in an attempt to minimize experimental scatter. In an exhaustive set of trials, f vs λ data were obtained which permitted the construction of a plot of phase velocity as a function of wave period. Using small amplitude wave theory the surface tension for this data was calculated to be 63 dyne/cm. A measurement of the static surface tension with a du Noüy tensiometer confirmed the low value of surface tension obtained from the dispersive relationship. The wavetank was cleaned and refilled with tap water. The static surface tension was measured and found to be 70 dyne/cm. From careful wavelength measurements and the small amplitude dispersive relationship the surface tension (dynamic) was calculated. A surfactant (Woolite) was added and the experiment was repeated. The static surface tension was measured with the tensiometer and found to be 30 dyne/cm, and again with in $\pm$ 1.5 dyne/cm the surface tension calculated from the dispersive relationship was in agreement. These experiments were taken to indicate that the correct value of surface tension could be obtained from either a measurement of the frequency and wavelength of the waves and use of the dispersive relation or by a simple static measurement of the surface tension. Similar results have been reported by Davies and Vose (1965) for most liquids including water; however, McGoldrick (1970) has reported values of the dynamic surface tension 10% lower than the static value for water. After this confirmation of the equivalence of results from either method the phase velocity was subsequently obtained from static surface tension measurements and direct computation using the dispersive relationship with periodic verification by direct measurements of the wave length.

Preliminary trials of the optical system consisted of the measurement of peak to trough amplitudes of arbitrarily selected gravity-capillary waves in the range of 6 to 18 Hz. The amplitude (computed as described in Sec. 3.1) as measured by the optical system was compared to the amplitude as measured by a capacitive wave height transducer similar to that developed by McGoldrick (1971). The present wave height transducer consisted of a No. 30 hypodermic needle (diameter 0.224 mm) which, when immersed in the water surface, controlled the amplitude of a 455 kHz square-wave oscillator. After suitable amplitude demodulation, an analog voltage proportional to the needle immersion depth was obtained. For the longer wavelengths (greater than approximately 5 cm) the two

systems had identical responses, but for shorter wavelengths the optical system indicated predominately higher values of peak to trough amplitude (c.f. Fig. 3-6).

To determine which instrument was in error a direct geometric measurement of wave amplitude was made. This was accomplished by using a sinusoidal surface wave which was obtained by adjusting the amplitude, frequency and position of the wave generator. For a sinusoid of peak to trough amplitude, a, the maximum slope is ak/2. The maximum angle swept by the refracted beam was determined by measuring with a scale the swept length of the beam on a plane a known distance from the water surface. The value of ak was then calculated from the relation

$$ak \doteq \text{swept length/distance of water to plane}$$

Then a measurement of wavelength, and thus k, permitted a separate measurement of amplitude for this special case. The amplitude measured in this manner closely agreed with that obtained by the optical system and this established the measured amplitude as a tentative standard.

With this standard, constant peak to trough amplitude surface waves were generated at varying wavelengths. A summary of the response is presented in Fig. 3-6.

In an attempt to explain the observed rolloff in the response of the wave height probe at the shorter wavelengths it was hypothesized that the meniscus did not maintain a constant height on the probe. Another way of expressing this is to say the meniscus exhibited a hysteresis effect and did not slide on the probe as if it were a rigid body. This hypothesis was investigated experimentally by the forced immersion of the probe into still water. While attached to the wave generator shaft (plunger wedge removed) the probe was driven with a number of waveforms, symmetrical and non-symmetrical, over a range of frequencies from 0.2 to 40 Hz at various amplitudes. Under all conditions imposed, the immersion depth as measured by the probe, compared within 10% to that of the wave generator shaft displacement as indicated by the dcdt position transducer. It was therefore concluded that the meniscus maintains a nearly constant height on the probe with respect to the instantaneous position of the level surface. The small attenuation observed was insufficient to explain the rolloff presented in Fig. 3.6.

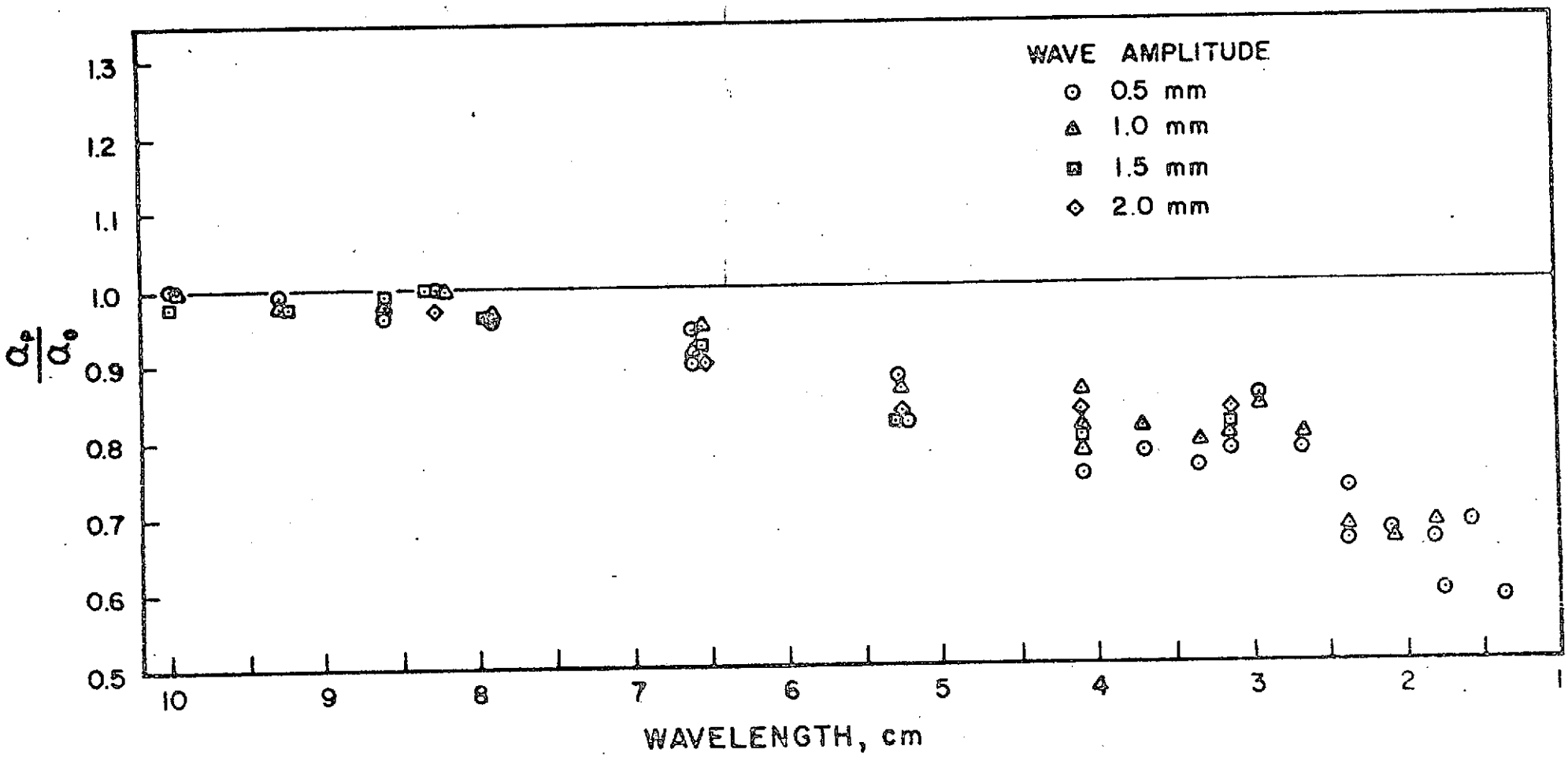

Figure 3-6. Ratio of wave amplitudes as measured by the probe (a_p) to that measured by the optical method (a_o). The light beam is 0.30 mm in diameter.

An alternate explanation for the reduced probe response at the shorter wavelengths was postulated to be a lack of spatial resolution. At the shorter wavelengths a higher degree of resolution becomes necessary to avoid an averaging of the amplitude structure. It was therefore hypothesized that if the effective size of the probe resulting from an attached meniscus was much larger than that of the unwetted probe, the resolution would be limited by this effective probe diameter. To check this hypothesis the diameter of the light beam was gradually increased from a nominal 0.5 mm to a diameter of approximately 6 mm. With this 6 mm beam diameter (and consequently reduced spatial resolution) the response of the optical system and the capacitive wave height probe were nearly identical. Figure 3-7 presents a plot of the ratio of peak to trough amplitudes as measured by the wave height probe to that obtained by the optical system.

Within the bounds of experimental error and the exception of a small unexplained dip in the probe response at λ = 2 cm, the two systems had a comparable response. It is therefore concluded that the observed rolloff of the wave height probe at short wavelengths was due to a lack of spatial resolution. For the No. 30 needle used the effective diameter of the attached meniscus was assumed to be that of the enlarged light beam and thus approximately 5-7 mm.

The problem of insufficient spatial resolution has been considered by Cox (1958) for his optical system. When one substitutes the experimentally determined effective probe diameter of 5-7 mm for the sensor diameter in his analysis a response which closely parallels the data of Fig. 3-7 is predicted.

A theoretical means of estimating effective probe diameters, and hence the resolution, can be obtained by an analysis of static menisci on circular cylinders. One observes from meniscus profiles, calculated numerically and verified experimentally by White and Tallmadge (1965), that an effective probe diameter of 6 mm would correspond to the diameter of the meniscus where the height is $\frac{1}{10}$ the maximum height. Using this criterion Table 3-1 presents calculated effective diameters for probes roughly double and half the diameter used in this investigation.

It is clear from Table 3-1 (and casual observations of probes in water) that the meniscus diameter is much larger than the probe itself. Since the effective sensor diameter presented by the meniscus is a rather weak function of probe diameter this points out that lack of spatial resolution is an

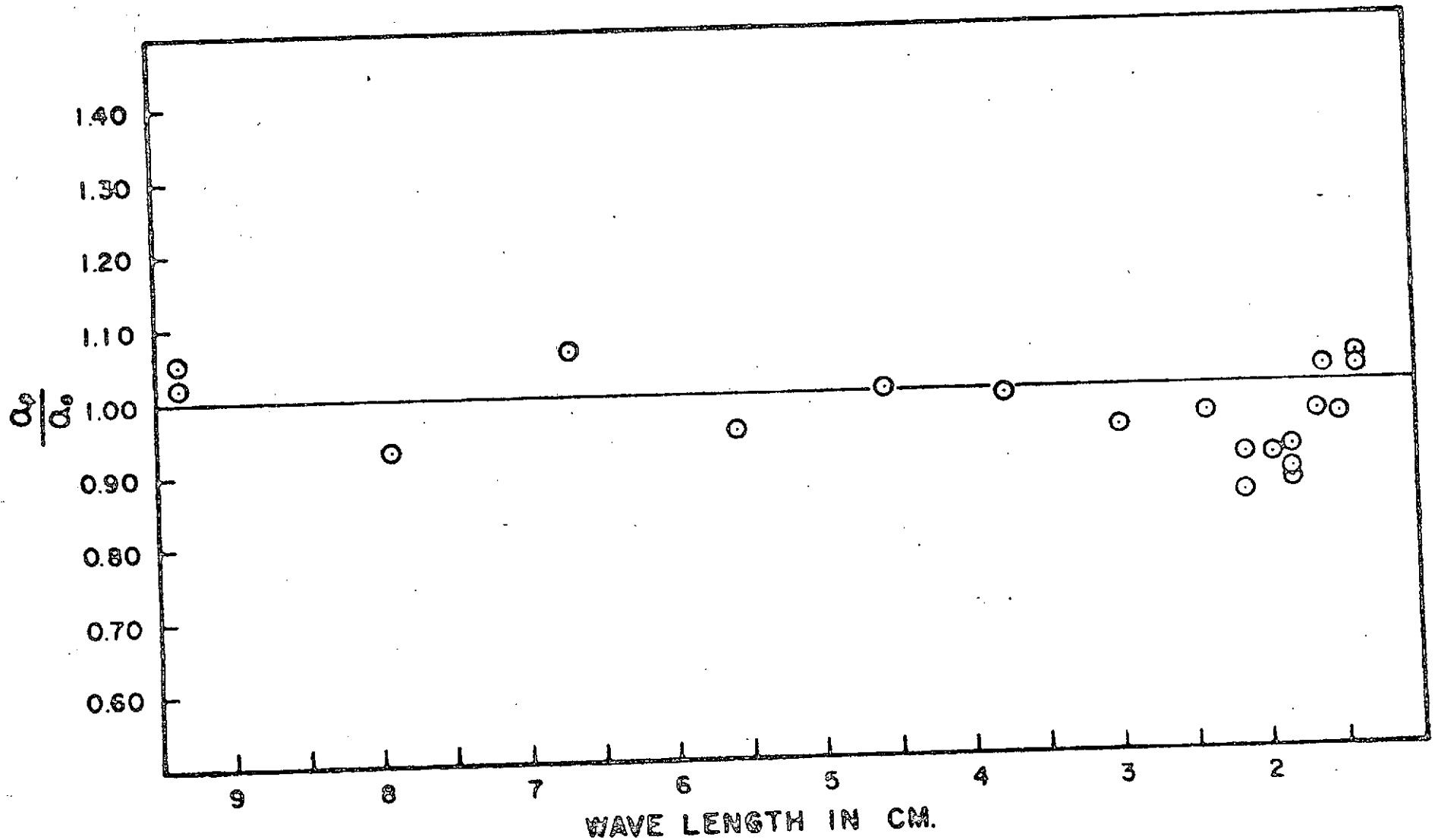

Figure 3-7. Ratio of wave amplitudes when the light beam diameter is 6 mm.

Actual probe diameter (mm)	Calculated effective probe diameter (mm)	
	T=70 dyne/cm	T=30 dyne/cm
0.50	6.5	5.0
0.224	5.7	3.9
0.10	2.7	2.0

TABLE 3-1. Actual probe sizes versus effective probe size.

inherent problem with this class of wave detectors. This would appear to be a serious restriction of the usefulness of these wave height probes where the measurement of small, short waves is desired.

In passing it must be noted that the optical system described responds to general two-dimensional surfaces as the light beam is refracted in relation to the total surface slope. As a consequence, when the refracted light beam is projected on a flat surface one visually observes a two-dimensional pattern, similar to a Lissajous figure, if a two-dimensional surface disturbance is scanned. For the special case of one-dimensional wave trains, the pattern degenerates to a straight line. When transverse waves are present the pattern opens into a two-dimensional figure. This feature is especially useful for detecting low amplitude cross (transverse) waves which are frequently observed to be associated with plunger type wave generators. In one-dimensional wave studies this form of distortion is much more difficult to detect with wave height probes.

Having established the calibration, we moved on to measure the decay rates of the energy density of two capillary waves. The rate of energy decay is calculated according to

$$\frac{dE}{dt} = \frac{1}{C_g}\frac{dE}{dX} = \frac{2\gamma k^2}{C_g} \qquad (3\text{-}19)$$

where γ is the surface tension force. The calculated and measured results are shown in Figures 3.8 and 3.9.

The final measurement using the present system was on current velocity. A pump was connected to the tank to generate a variable current anywhere between $\pm$ 20 cm/sec. The current velocity was independently measured by a hot film anemometer and three sets of test were conducted with two of the tests for waves traveling with the current and one for waves travelling against the current. The results are summarized in Tables 3-2, 3-3, and 3-4.

3.4 Additional Laboratory Work

Since the final test of the theory will not be conducted in the capillary wave range alone, a wind-wave channel with the dimensions of 2' x 3' cross-section and 50' long has been constructed through the coastal research program supported by the North Carolina State Government at NCSU. The blower on the

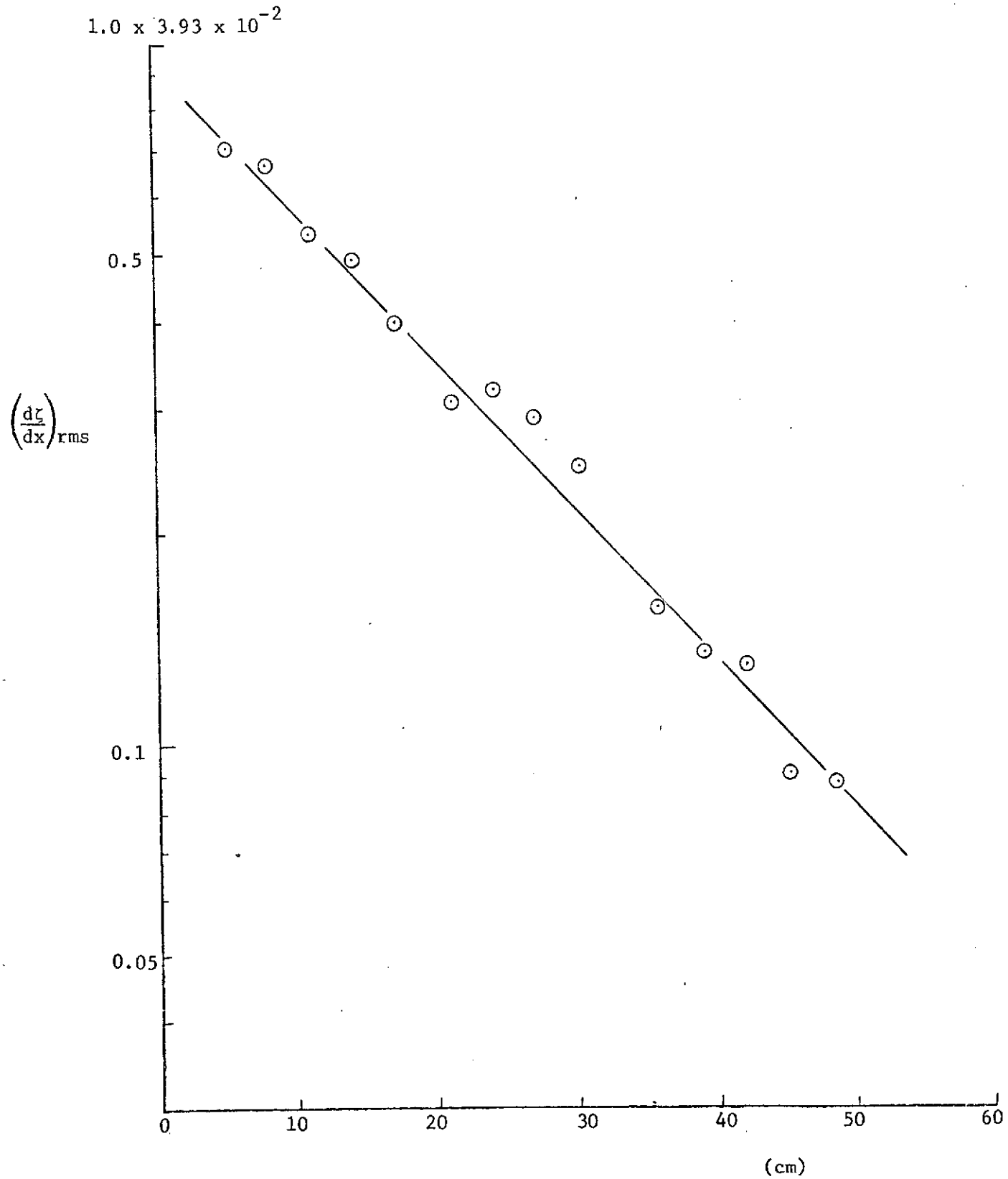

Figure 3-8. Capillary wave energy decay as a function of distance under current. $K = 7.23\ cm^{-1}$, $\sigma = 108.04\ sec^{-1}$, $U = 10.5$ cm/sec. ——— indicates theoretical calculated value, ⊙ observed values.

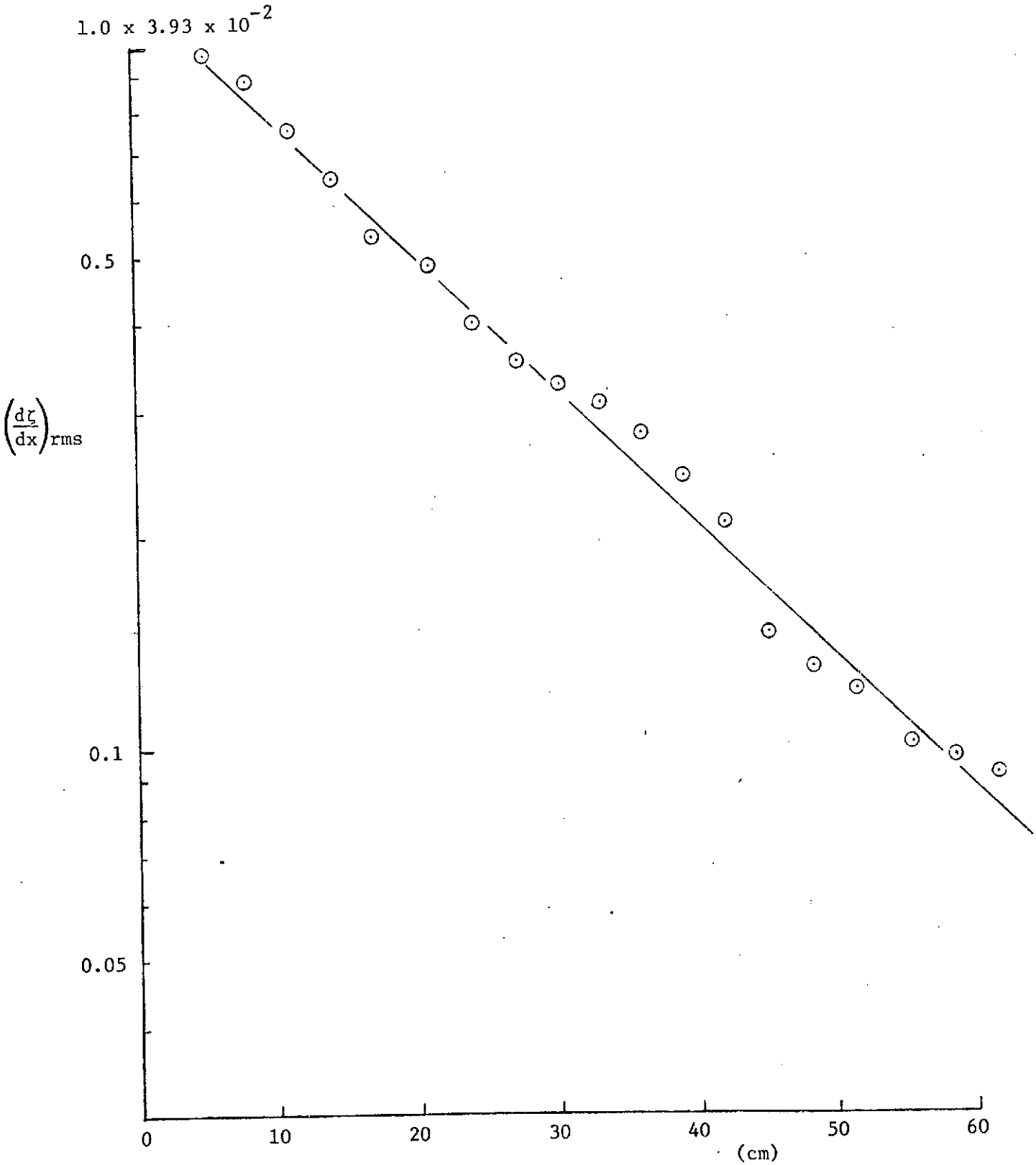

Figure 3-9. Capillary wave energy decay as a function fo distance under current. K = 6.37 cm^{-1}, σ = 78.80 sec^{-1}, U = 12.37 cm/sec. —— indicates theoretical calculated value. ⊙ observed values.

Measured		Calculated		$\frac{U_{measured}}{U_{calculated}}$
Period (ms)	Wave length (cm)	Current (cm/sec) $U_{calculated}$	Current (cm/sec) $U_{measured}$	
24.860	0.878	11.0	9.89	1.112
24.866	0.903	10.0	11.06	0.904
24.868	0.924	11.5	12.08	0.961
24.864	0.859	9.0	8.98	1.002
28.575	0.993	11.5	10.15	1.133
28.574	0.999	12.0	10.37	1.157
28.635	0.972	12.0	9.23	1.300
28.606	1.010	14.0	10.84	1.292
28.604	0.998	11.0	10.30	1.068
25.125	0.860	11.0	8.66	1.270
25.358	0.927	11.5	11.50	1.000
25.905	0.932	11.5	11.76	0.978

Average = 1.097

TABLE 3-2. Current measurements through wave kinematics Case 1.

Measured			Calculated	$U_{measured}$ / $U_{calculated}$
Period (ms)	Wave length (cm)	Current (cm/sec) $U_{measured}$	Current (cm/sec) $U_{calculated}$	
27.970	0.984	11.5	10.53	1.092
24.940	0.883	11.5	10.02	1.148
23.318	0.836	10.0	10.04	0.996
21.420	0.768	9.5	9.37	1.014
28.016	0.964	9.0	9.65	0.941
27.880	0.966	9.0	9.92	0.907
35.590	1.186	9.0	9.63	0.935
30.470	1.007	9.0	8.52	1.056
27.276	0.942	9.5	9.62	0.988
28.507	0.903	5.0	6.44	0.776
31.000	0.940	5.0	5.36	0.933
32.570	1.116	10.2	10.30	0.991
29.199	0.989	10.5	9.25	1.135
26.359	0.910	9.0	9.33	0.965

Average = 0.991

TABLE 3-3. Current measurements through wave kinematics Case 2.

Measured			Calculated	$\frac{U_{measured}}{U_{calculated}}$
Period (ms)	Wave length (cm)	Current (cm/sec) $U_{measured}$	Current (cm/sec) $U_{calculated}$	
62.170	0.757	-14.5	-14.33	1.012
66.440	0.982	- 9.0	- 9.89	0.910
58.820	0.894	- 9.0	-10.10	0.882
55.300	0.859	- 9.0	-10.00	0.900
62.170	0.695	-14.5	-16.24	0.893
62.195	0.941	- 8.5	- 9.80	0.867
66.621	0.859	-11.5	-12.69	0.906
58.825	0.925	- 9.0	- 9.32	0.965
55.325	0.854	-10.0	-10.17	0.983
58.159	0.869	-11.0	-10.55	1.043
58.158	0.735	-14.0	-14.25	0.982
58.159	0.826	-11.0	-11.70	0.940
66.441	0.900	-11.0	-11.70	0.940
80.415	0.986	-11.5	-12.38	0.929
99.612	1.143	-11.5	-12.38	0.929
100.627	1.143	-11.5	-12.51	0.919
100.573	1.522	- 8.0	- 7.90	1.013
75.648	1.165	- 8.0	- 8.39	0.954
54.702	0.918	- 8.0	- 8.31	0.963
54.590	0.926	- 8.0	- 8.08	0.990

Average = 0.990

TABLE 3-4. Current measurements through wave kinematics Case 3.

tank is capable of generating a wind up to 80 knots. A variable speed pump will be connected to the tank to generate current together with wind and waves. This channel will be used to check the theoretical results in a near natural environment. Since wind waves are highly irregular, cross tank components will become increasingly important. The waves will be quasi-two-dimensional. Under this condition, the present system described in Sections 3.1 and 3.3 will become inadequate, and a new electronic system is being designed and constructed in our laboratory. The construction is still unfinished at the present moment. The detail of the system is described as follows.

To analyize the two-dimensional signal resulting from the wind-wave field, an array of light sensitive diodes was used, thirty-two Vactec S150LB diodes for each dimension, allowing two diodes for each of the sixteen steps in each dimension as shown in Figure 3-10. Since the laser beam is, at any one instant of time, a single dot, only one strip at a time in each array will be illuminated by the dot. The location of the dot gives the slope in x and y directions respectively. As the dot moves, there will also be times when the dot crosses the gap between strips of diodes. Thus the electrical output from each array will be a burst of voltage, typically about 70 mv, when the dot of light is on any given diode, with zero output for the gaps between the strips. To convert this output into data that are more readily analyzed, an array of integrated circuits was employed.

Initially, thirty-two voltage comparators, MC1710, are divided into two groups of sixteen. Each of the sixteen monitors one of the arrays of diodes and each strip in the array is therefore continuously monitored for output. The function that the MC1710 comparators perform is to compare voltages with a reference voltage that is adjustable by means of a 10K Ohm trim pot and each is therefore tuned to the output level of its particular pair of diodes on the strip it monitors. The typical output differs slightly from 70 mv due to diode manufacturing variations, thus each comparator is tuned to recognize the dot when laser light strikes the diode strip and causes a voltage greater than its reference. The comparator then switches "on", supplying one NAND gate in a N7400A package with about 3.2 volts. The NAND gate inverts the signal and switches on one of the FLIP-FLOPS in a dual package, US7476A.

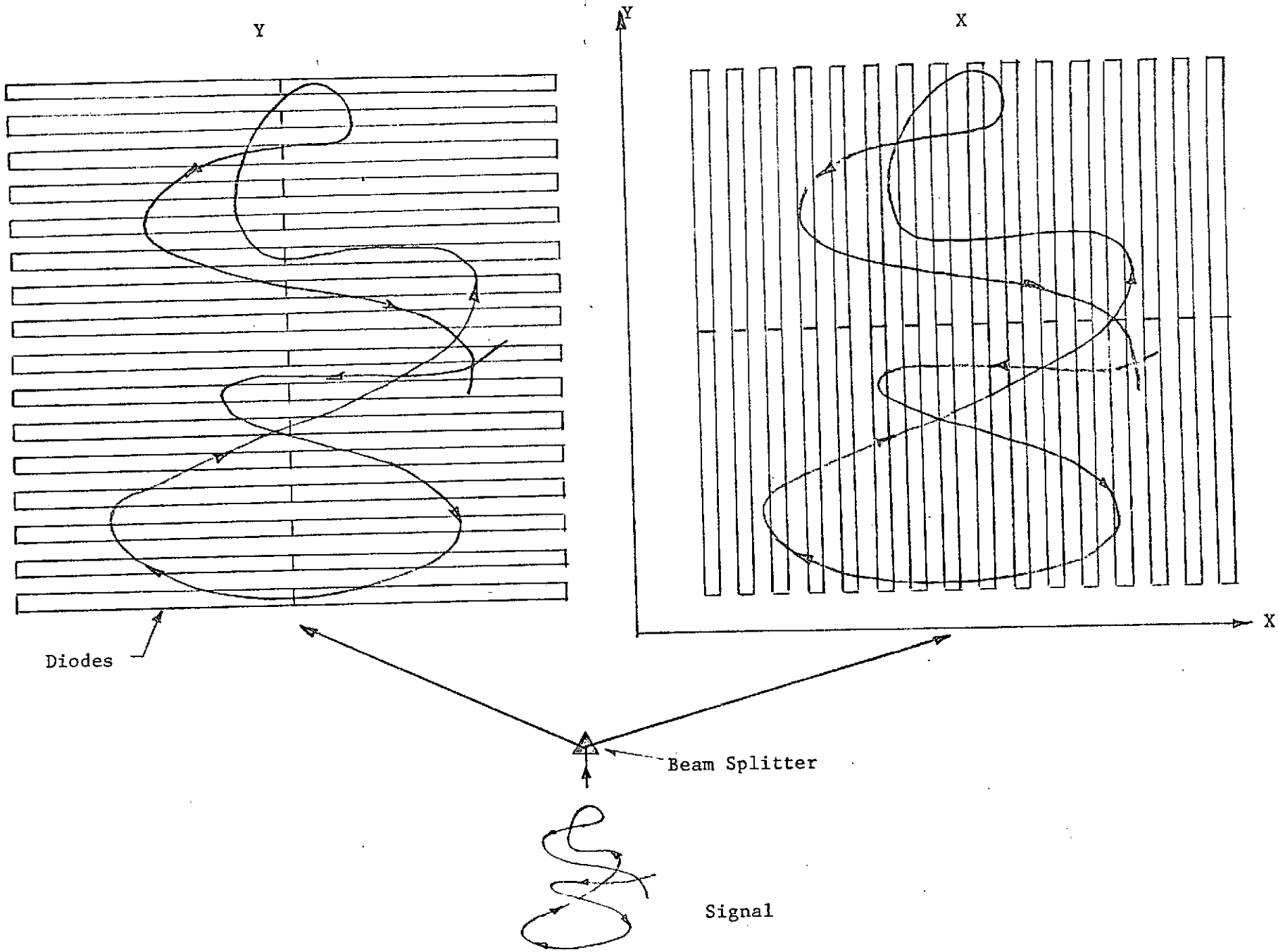

Figure 3-10. Arrangement of the Photo diodes for two-dimensional waves.

Unlike the comparators or NAND gates, the FLIP-FLOPS will remain "on" supplying about 3.5 volts until instructed to turn "off". This feature of the FLIP-FLOPS enables the final output to remain at that level while the dot crosses the gaps between strips, and no incoming signal is present. To prevent more than one FLIP-FLOP in each array division from being on at the same time (which would indicate the dot was at two places at the same time), part of the initial output of the FLIP-FLOP turns on a NOR gate, in a N7402A package, which in turn switches "off" (through the reset input) the FLIP-FLOPS corresponding to the step on either side of the location of the dot. Thus the final output of the FLIP-FLOP corresponds to the location of the laser dot on the diode. Since all the FLIP-FLOP outputs are the same, typically 3.5 volts, these outputs are fed through precision resistors changing in value from 2K to 16K in 1K steps. Each 1K step corresponds to a different diode strip, and thus when fed into a MC1741 OP AMP, are amplified differentially. The final output then appears as "steps" in close approximation to the continuous slope. For smaller steps, and thus more accuracy, only the addition of more diode strips and electronics to monitor them is necessary. To summarize the description, the original quantized output of the diodes is processed electronically into slope information as shown schematically in Figure 3.11. To make this electronic analysis of the signal, the following supply voltages were needed:

MC1710	Comparators --- + 14v, - 7v, 80 mv reference	
N7400A	QUAD 2-INPUT NAND GATE	+ 5v
US7476A	DUAL J-K FLIP-FLOP	
N7402A	QUAD 2-INPUT POS. NOR GATE	
MC1741	OP AMP	$\pm$ 15v

To supply these voltages, an MC1561R was used for the $\pm$ 15v and 80 mv, another MC1561R for the + 14v and MC1463R for the - 7v, and a ZN3055 power transistor working with a 1N4733 Zener diode for the + 5v. A detailed circuit diagram is given in Figure 3.12.

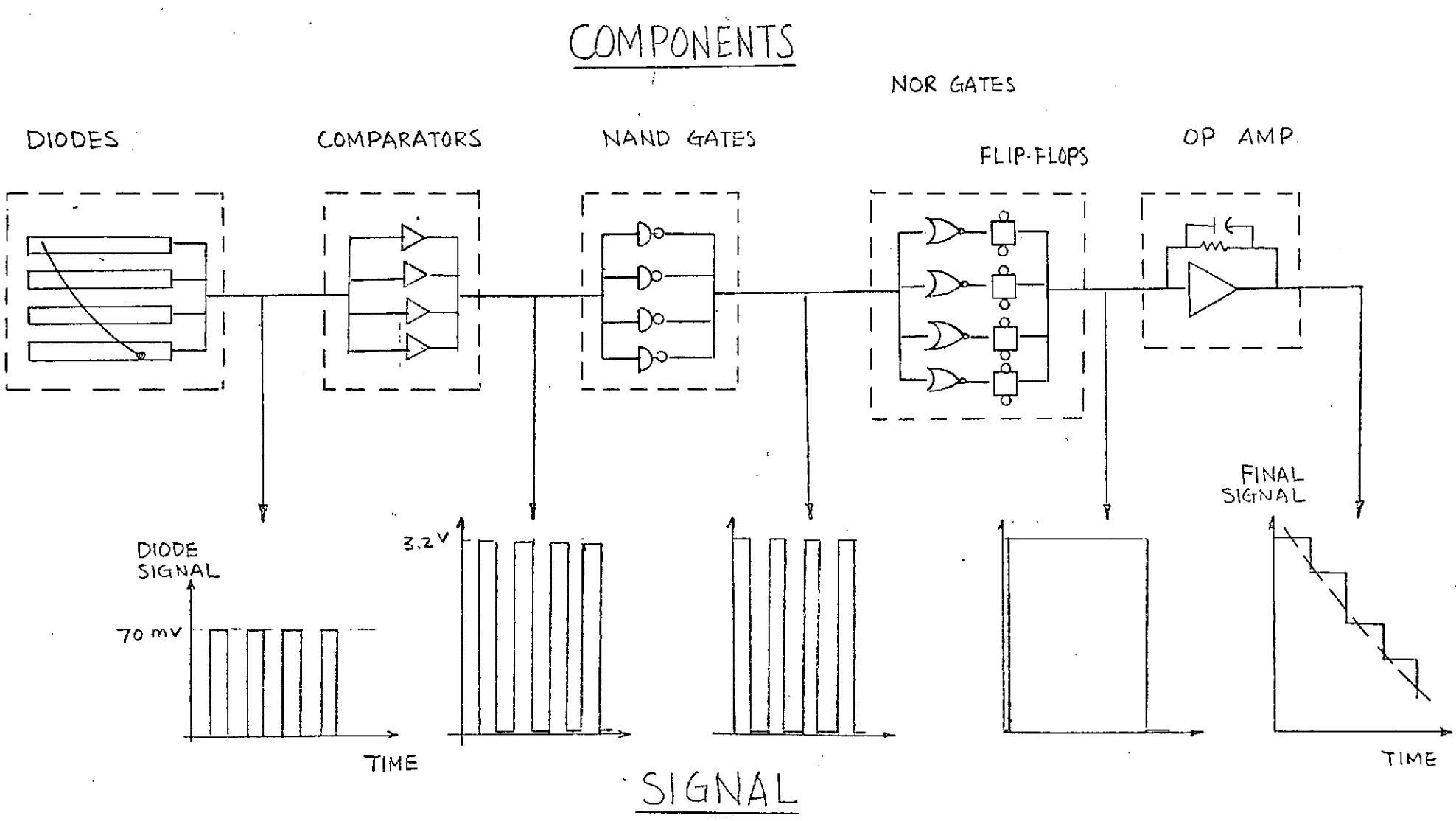

Figure 3-11. Schematic diagram of the signal processing.

FOLDOUT FRAME 1

FOLDOUT FRAME 3

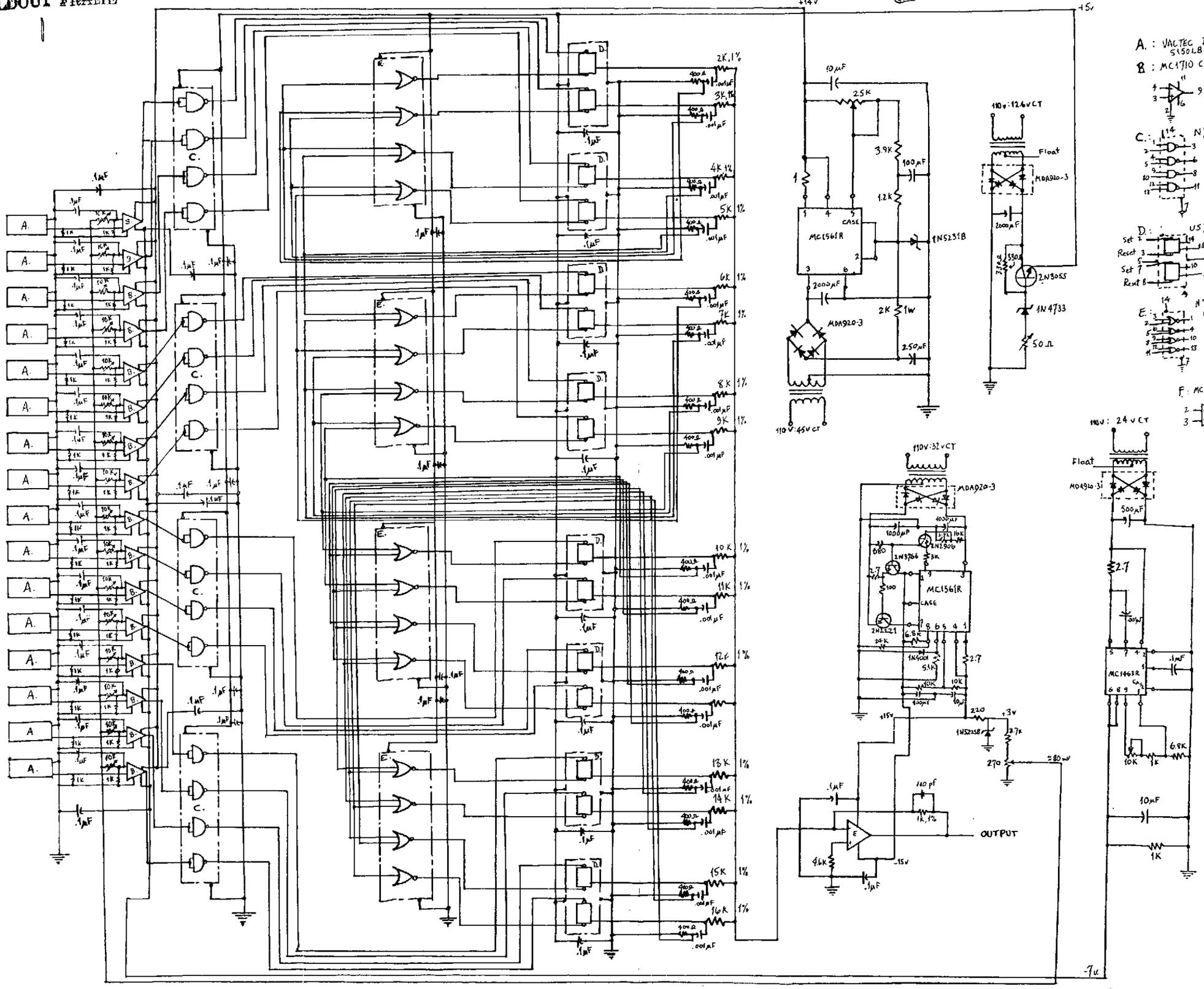

Figure 3-12. Circuit diagram for the two-dimensional wave sensor.

4.0 SUMMARY AND DISCUSSION

The feasibility of monitoring surface current through wave observation by remote sensing technique was established in theory and also in preliminary experimental tests. The accuracy of the method, under laboratory controlled condition, is comparable to any other in situ measurements. Two different approaches were discussed. For the experiment, the kinematic approach was verified for a single train of gravity-capillary waves. The final decision for field adoption will, of course, depend on the kind of instruments available at that time.

For the laboratory studies, an optical wave slope detection system capable of fine spatial resolution and high frequency response has been developed. The system, which employs the refraction of a narrow beam of light at the air-water interface, is ideally suited to the study of short gravity-capillary waves ($\lambda < 5$ cm) as spatial resolution is controlled by the light beam diameter, frequency response by the electronics employed, and no extraneous surface distortion is generated. For the special case of a single train of waves propagating with a known phase velocity, the slope signal can be integrated (electronically in the present case) to obtain the wave amplitude as it passes a fixed observation point. Moreover, the technique is applicable to the study of waves on a current, providing the total phase velocity (in laboratory coordinates) is used in the slope to amplitude calculations. The accuracy of the present amplitude measurement technique is largely dependent on the accuracy to which the phase velocity is known. Experiments indicate that the surface tension calculated from measurements of wave frequency and wavelength agree to within $\pm$ 1.5 dyne/cm with that measured by a du Noüy tensiometer, and thus small amplitude wave theories can be used to calculate phase velocity once the (static) surface tension has been measured. In the absence of a "standard laboratory wave" the overall accuracy of the optical slope/amplitude detection system must be estimated from the total instrumentation uncertainty. For the measurement of waves with peak slopes less than 0.5 the present system should give wave slopes accurate to within 5%. The total amplitude error is that of the combined slope and integrator error multiplied by the uncertainty in the phase velocity. For the present investigation this total error is estimated to be less than 10%.

Although the preliminary results are encouraging, considerably more work remains until an operational routine can be established. In order to achieve such an ultimate goal, the following studies have to be carried out.

(a) Additional Theoretical Analysis

The theoretical study will be used as a guide for planning both in the laboratory and in the field. The more we know about the topographical features of a random wind-wave field, the more we can detect the influence of current on waves. The theoretical studies will include both kinematics and dynamics of wind generated waves over all wave number-frequency range. Although in the ocean most energy is contained in the gravity wave range which has also held the central attention of oceanographers, the gravity-capillary waves or even the pure capillary waves are important in radar remote sensing problems.

(b) Additional Wave Tank Studies

A wave tank study is the first step prior to field tests. In order to simulate the natural environment better, wind generated waves will be used next. The two-dimensional wave sensor will be employed to make wave spectrum analysis. Such observations can be used to check the validity of theoretical results and also provide guidance for field instrument design.

Table 4-1 is given as a summary of the status of the study. Completed, planned and in-progress efforts are listed for quick reference.

TABLE 4-1. Summary of work in progress and future plans.

	GRAVITY WAVES		GRAVITY-CAPILLARY WAVES		CAPILLARY WAVES	
	REGULAR	RANDOM	REGULAR	RANDOM	REGULAR	RANDOM
THEORETICAL STUDY	EXISTING	FINISHED 2D, 1D } current PLANNED RANDOM CURRENT	FINISHED KINEMATIC PLANNED DYNAMICS	PLANNED	IN PROGRESS 2-D, 1-D } currents	IN PROGRESS 2D, 1-D } current
EXPERIMENTAL STUDY	EXISTING	PLANNED	IN PROGRESS 1-D current	PLANNED	IN PROGRESS (1-D current)	PLANNED

REFERENCES

Cox, C. S. (1958):
Measurements of Slopes of High-Frequency Wind Waves
(J. Mar. Res., 16, 199-225)

Cox, C. S. and Munk, W. H. (1954)
Measurements of the Roughness of the Sea Surface from Photographs of the Sun's Glitter
(J. Optical Soc. Amer., 44, 838-850)

Davies, J. T. and Vose, R. W. (1954)
On the Damping of Capillary Waves by Surface Films
(Proc. Roy. Soc., A, 286, 218-234)

Francis, J. R. D. and Dudgeon, C. R. (1967)
An Experimental Study of Wind Generated Waves on a Water Current
(Q. J. Roy. Meteor Soc., 93, 247-253)

Huang, N. E.; Chen, D. T.; Tung, C. C. and Smith, J. R. (1972)
Interactions between Steady Non-uniform Currents and Gravity Waves with Applications for Current Measurements
(J. Phys. Oceangraphy, 2, 420-431)

Hulburt, E. D. (1934)
The Polarization of Light at Sea
(J. Optical Soc. American, 24, 35-42)

McGoldrick, L. F. (1970)
An Experiment on Second-Order Capillary Gravity Resonant Wave Interactions
(J. Fluid Mech., 40, 251-272)

McGoldrick, L. F. (1971)
A Sensitive Linear Capacitance-to-Voltage Converter, with Applications to Surface Wave Measurements
(Rev. Scientific Inst., 42, 359-361)

Phillips, O. M. (1966)
The Dynamics of the Upper Ocean
(Cambridge University Press, pp. 261)

Plate, E. and Trawle, M. (1970)
A Note on the Celerity of Wind Waves on a Water Current
(J. Geophys Res., 75, 3537-3544)

Schooley, A. H. (1954)
A Simple Optical Method for Measuring the Statistical Distribution of Water Surface Slopes
(J. Optical Soc. Amer., 44, 37-40)

White, D. A. and J. A. Tallmadge (1965)
Static Menisci on the Outside of Cylinders
(J. Fluid Mech., 23, 325-336)